Desalination and Water Treatment
www.deswater.com
doi: 10.1080/19443994.2013.800251

52 (2014) 3035–3046
April

Taylor & Francis
Taylor & Francis Group

Water entropy-driven electrochemical relaxation of dissolved oxygen in aerated refinery wastewater

Mirjana M. Ševaljević[a,*], Miroslav M. Stanojević[b], Stojan N. Simić[c], Miladin V. Ševaljević[d]

[a]*High Technical School, and T.F."Mihajlo Pupin, in Zrenjanin University of Novi Sad, Serbia*
Email: sevaljevic.mirjana @gmail.com
[b]*Faculty of Mechanical Engineering, University of Belgrade, Serbia*
[c]*Oil Refinery a.d. Modriča, Bosnia and Herzegovina*
[d]*High Technical School in Zrenjanin, Serbia*

Received 27 September 2012; Accepted 21 April 2013

ABSTRACT

The results obtained in this paper show dissolved oxygen monolayer chemisorptions in gas bubbles in aerated and saturated refinery wastewater is water entropy-driven relaxation processes. Dissolved oxygen and hydrogen electrons affinity keep constant liquid water molecules entropy. In the time period of water molecules crystallization on water input, or volatilization on air output on active adsorption or condensation nucleuses depending on aeration regimes, oxygen adsorption heat keeping constant liquid water entropy enabling coupling with positive or negative hydrated hydrides entropy change. The relationship between oxygen monolayer adsorption heat to Langmuir adsorption isotherm and oxygen diffusion transfer energy after saturation time are found on the basis of previously obtained experimentally data (temperatures and stationary oxygen concentrations). In this paper, the energy efficiency depending on oxygen entropy level and oxygen total energy level between drift and saturation time period is also examined.

Keywords: Membranes air distributor; Chemisorbed oxygen; Entropy driven process; Entropy level; Oxygen energy level; Technical characteristics

1. Introduction

The intention of this paper is to examine water entropy-driven electrochemical relaxation processes, on the basis of experimental data obtained in previous papers [1–4], depending on aeration regimes and membrane distributor characteristics.

In our previous investigations, water aeration was performed in the procedure using experimental installation, a polypropylene column aeration tank with membranes air diffuser (PP GF30), to obtain technical characteristics of aeration systems described also in literature [7–12] influencing on efficient purification of the real sample with added waste oil content of 5 and 10 mg/L [13,14].

The presence of impurities in refinery wastewater, active adsorption, or condensation centers with small radius produce strong electric fields of water monolayer solvated electron $e{\cdot}H_2O$ and stream of particle with kinetic energy 300–500 kJ [5]. Then, adsorbed hydrogen dissociation energy will be generated producing unusual ions and radicals, semi-conductor

*Corresponding author.

metal oxide generates various oxygen species, O_2^-, O^- or O^{2-}. Reversible reactions with certain gases minimize the free energy of the system by formed points, lines, layers, or composites going to be periodic in arrangements [6]. Electron motion being prompted by the fluctuating electrostatic field of solvent where there is rapid displacement between H atoms, characterized by a free energy barrier of k_BT dependent on the position and orientation of surrounding water molecules [15–21].

According to the literature [15], diffusion activation energy of hydrated electron in liquid give much larger experimental value at around 20 kJ/mol compared to computational model, 8–10 kJ/mol for diffusion coefficient 0.49 nm^2/ps, twice times faster than water self-diffusion coefficient 0.23 nm^2/ps. Mechanism of increased electrons conduction indicated charge transfer provides a significant contribution to the overall migration of the charge by the diffusion of hydrated electron involving the exchange of an extra molecular electron between identical solvent molecules or solvated indicators, S [15]:

$$[O_2 \cdot e \cdot aq] + S \rightarrow O_2 + [S \cdot e \cdot aq] \quad (1)$$

On the basis of experimental data obtained in our previous investigations of aeration regimes, water column 1 and 2 m high at air flows 2, 6 and 10 m^3/h without addition and after addition of 5 and 10 mg/l waste motor oil in real sample of refinery waste water, in this paper is examined for oxygen adsorption equilibrium constant influence on diffusion activation energy.

2. Experimental

Experimental work was performed for batch working conditions and varying air flow of 2, 6, and 10 m^3/h. Average characteristic of wastewater in Refinery in Modriča, in period of investigation were: pH in range 7–8, temperature 15–25°C, oil content 13–23 mg/L, inorganic salts 0.38–0.40 mg/L, TSS 0.5–0.7 mg/L, HPK 80–180 mg/L, BPK up to 0–7 mg/L, CaO 18.5–21.5 mg/L, and electric conductivity 670–770 μS/cm. Characteristics of wastewater in the range of 992–996 kg/m^3, viscosity in range of 0.81×10^{-6}–0.99×10^{-6} m^2/s, and surface tension coefficients were 76.2, 64.8, and 57.3 mN/m, respectively. The water level in the column was 1 and 2 m high and the total volume was 490 and 980 L. Water aeration with the real sample and with added waste oil content of 5 and 10 mg/L was performed to enable examined water are dependent of the added viscous waste motor oil (SAE 15W-40, with 132.0 mm^2/s viscosity index, with inflammation temperature 231.0°C, with 3.18 mg KOH/g TAN, as 9.73 mg KOH/g TBN, with content of 0.039% Zn, 0.310% Ca, 13.4 ppm Fe, 4.11 ppm Cu, 0.98 ppm Cr and 44.87 ppm Al). Densities of three examined samples of water were in range of 992–996 kg/m^3, viscosity in range of 0.81×10^{-6}–0.99×10^{-6} m^2/s, and surface tension coefficients were 76.2, 64.8, and 57.3 mN/m, respectively. The water level in the column was 1 and 2 m high and the total volume was 490 and 980 L. Water aeration with the real sample and with added waste oil content of 5 and 10 mg/L was performed to enable efficient purification [13,14].

Dissolved oxygen was previously removed using a chemical method. Air flow regulation is performed using a flow regulator and relieving valve, until a set value for the adopted investigation regime is attained. Air flow is stabilized at over-pressure value before distributor and orifice plate when the first air bubble entered in the water. Water sampling from the column in equal time intervals starts ($\Delta\tau = 60$ s) and the dissolved oxygen content is measured ,until the same value is repeated thrice (see Fig. 1).

3. Relationship between oxygen monolayer adsorption heat to Langmuir adsorption isotherm and oxygen diffusion energy

Previously determined oxygen adsorption rate constants [3] enable in this paper desorption rate constant to be calculated on the basis of oxygen adsorption equilibrium constants after chemical potentials, μ in contact surface between gas and liquid phase achieve equilibrium value:

$$\mu(O_2)_g = \mu(O_2)_l \quad (1a)$$

In this paper according to Langmuir adsorption isotherms to Eq. (2) are obtained:

- oxygen adsorption equilibrium constants (ratio between adsoption and desorption rate constants):

$$K_{Lg} = \frac{k_a}{k_d} \quad (1b)$$

- molar chemisorbed oxygen monolayer volume:

$$V_{mn}^{\theta} = \frac{1}{c_{\max}} \quad (1c)$$

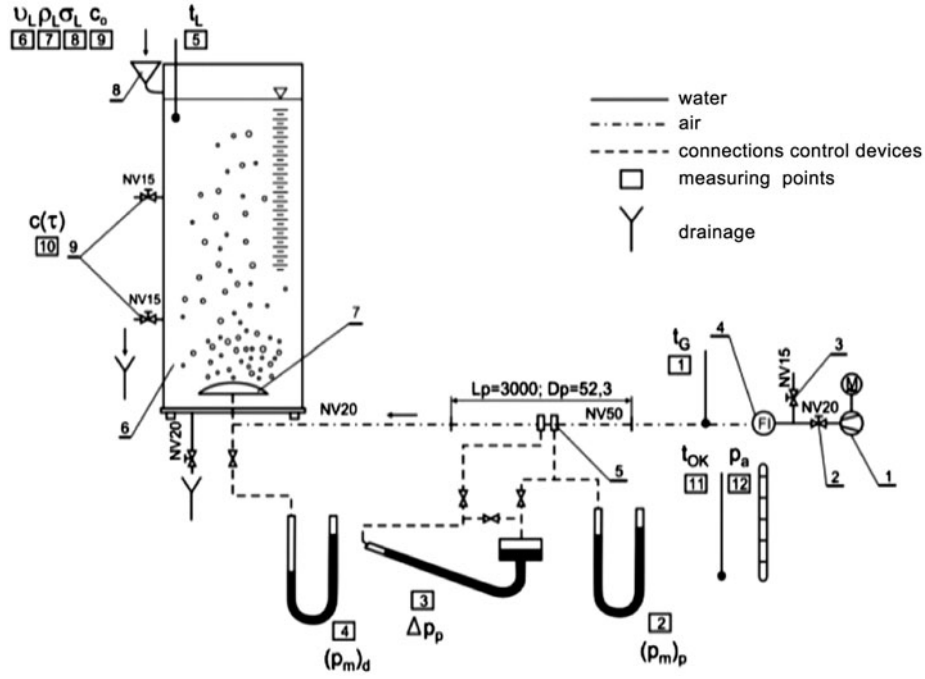

Fig. 1. Scheme of experimental installation [1–4]. (1) Low pressure compressor (blower); (2) valve on the air inflow pipe; (3) relieving valve; (4) air flow regulator; (5) air flow measuring orifice plate; (6) column with corresponding connections and framework; (7) disk-shaped membrane air distributor; (8) water supply; and (9) sampling connection.

On the basis of experimental data obtained and calculated in equilibrium of oxygen chemical potential between gas and liquid phase (Tables 1 and 2) depending on aeration regimes in previous papers [3,4], these values are calculated (Fig. 2, Tables 2 and 3) according to Langmuir adsorption isotherm Eq. (2):

$$\frac{1}{c(O_{2,ch})_g} = \frac{1}{c(O_2)_{\max}} - \frac{1}{K_{Lg}c(O_2)_{\max}} \cdot \frac{1}{c(O_2)_l} \tag{2}$$

$$y_o = \frac{1}{c(O_2)_{\max}} = V_{mn}^{\theta} \tag{2a}$$

$$\frac{y_o}{tg\alpha} = K_{Lg} \tag{3}$$

$$\Delta_{Lg}S^{\theta}(O_{2,ch}) = \frac{RT\ln K_{Lg}}{T} = R\ln K_{Lg} \tag{4}$$

Experimentally found oxygen adsorption heat (Fig. 2) calculated on the basis of equilibrium oxygen adsorption constant determined to Langmuir adsorption isotherm agree to the oxygen diffusion activation energy [3], after saturation period:

$$-T_l R\ln K_{Lg} = F\eta_d(O_2)_s \tag{5}$$

The relationship between experimentally found oxygen adsorption heat and oxygen diffusion transfer energy agree to literature defined hydrated electron diffusion activation energy [15] as much larger experimentally value at around 20 kJ/mol, compared to faster successive process defined to computational model 8–10 kJ/mol.

Table 3 presents the liquid water entropy change as difference between total entropy determined to Langhmuir adsorption isotherm and liquid water entropy:

- The positive entropy change of 2, 4 J/molK of produced most mobile components on condensation cemters in aeration regimes, $c{-}1{-}q$.
- the negative entropy change of at least mobile components on adsorption centers depending on aeration regimes (-3, 3 J/molK in $c{-}2{-}q \leqslant 6\,m^3/h$ and -1 J/molK in aeration regimes, $c{-}2{-}q = 10\,m^3/h$).

On the basis of previously calculated passive rate constants in the paper [3], the better correlation coefficient, $R^2 = 0.9181$ for adsorption rate constant are obtained in comparison with diffusion and chemical

Table 1
Oxygen diffusion energy transfer in water double film in gas phase in contact surface on the base previous calculated equilibrium of chemical potentials [3] used in this paper to obtain Langmuir adsorption isotherm—added motor oil content, c, mg/l ; water column height, h, m and air flow, q, m^3/h) [1,2]—stationary diffusion oxygen energy in liquid, $F\eta_{d,l} = RT\ln(O_2)_L$ [3]—molar adsorption oxygen affinity, ΔG^{θ} $(O_2)_{g/l}$ [3]—molar volume of chemisorbed oxygen in gas phase, V^{θ} $(O_{2,ch})_G = 1/c_a(O_{2,ch})_G$ [3] surface active monolayer volume, V_r^{θ}, dm^3[4]

c–h–q	$RT\ln c$ $(O_2)_g$, kJ/mol	V^{θ} $(O_{2,ch})_g$, dm^3/mol	$\Delta_{el}G^{\Theta}$ $(O_2)_{g/l}$, kJ/mol	V_r^{θ}, dm^3
0–2–2	10.58	5.00E+10	+30.4	+14.76E–3
	−56.16		−36.3	
0–2–6	10.58	5.00E+10	+30.4	,,
	−56.16		−36.3	
0–2–10	0.58	3.60E+255	+30.4	,,
	−1.398.2		−1.377	
5–2–2	−94.75	6.40E+21	−74.5	−7.04E–3
5–2–6	−84.02	3.57E+19	−64.2	,,
5–2–10	−56.16	5.60E+267	−64.2	,,
	−1.400		−1.377	
10–2–2	−84.72	3.57E+22	−64.2	−3.4E–3
10–2–6	−84.72	3.57E+22	−64.2	,,
10–2–10	−90.94	1.00E+274	−70.6	,,
	−1.398.7		−1.377	
5–1–2	−94.71	6.40E+21	−74.5	−7.04 E–3
5–1–6	−66.67	5.50E+14	−36.3	,,
5–1–10	−95.01	6.40E+21	−74.5	,,
10–1–2	−91.2	2.86E+20	−70.6	−3.4E–3
10–1–6	−91.2	2.86E+20	−70.6	,,
10–1–10	−91.2	2.86E+20	−70.6	,,

saturation rate constants, $R^2 = 0.5$–0.6 (see Fig. 3, Table 4).

According to the mechanism of increased electrons contribution to the overall migration of the charge, by a diffusion of hydrated electron involving the exchange of an extra molecular electron between identical solvent molecules or solvated indicators (S), according to literature [15], equilibrium adsorption constant to Langmuir adsorption isotherm can be defined according to our previous paper [4]:

$$K_{Lg} = \frac{[e] \cdot ([O_2]^* - [O_2]_s)}{[O_2]^*} \tag{5a}$$

On condensation or crystallization nucleuses the new oxygen energy level in presence of the most mobile adsorbed H^+ ions is defined enabling electrochemical oxygen equilibrium to be achieved, with most mobile adsorbed particles [4]:

$$-\Delta\mu(O_2/OH^-) = F\Delta E(H^+ + e/1/2H_2)_g = FE_{ind}^{\theta} \tag{5b}$$

According to Langmuir adsorption isotherm coupled electrons and oxygen diffusion transport c explain experimental obtained results, based on Eq. (1) [15]:

$$O_2 + e + H^+ + S = O_{2,ad} \cdot S$$

In our previous paper [4] significant correlations were obtained depending on aeration regimes for:

(1) the calculated electron density in specific monolayer volume.
(2) electrochemical hydrogen potential defined to Nernst law enabling oxygen over-pressure isothermal isobaric relaxation, in contact surface between with fastest adsorbed gas hydrogen, $\Delta p(O_{2)}) = \Delta p(H_2) = \Delta p(air)_{input}/5$:

$$\varphi_{H_2} = E_{ind}^{\theta} = \frac{RT_G}{F}\ln\frac{[e]_{couple}}{\sqrt{\Delta p(H_2)}} \tag{5c}$$

Table 2
Experimental data for oxygen concentration in liquid phase and liquid temperature [2] and oxygen diffusion transfer energy in water double film in liquid phase, as well as equilibrium adsorption constant and adsorption heat calculated to Eq. (2) according to Fig. 2—oxygen stationary concentration in liquid, c_s [2]—stationary oxygen diffusion energy transfer in liquid, $RT\ln c(O_2)_l = F\eta_{d,1}$ [3]—oxygen adsorption equilibrium constants to adsorption Langmuire isotherm, K_{Lg}, acc. to Fig. 2—oxygen adsorption heat in liquid phase released at stationary liquid water entropy, $-T_l R\ln K_{Lg}$

c–h–q	t_L, ℃	c_s, mg/ l	$F\eta_d$ $(O_2)_s$, kJ/mol	K_{Lg} Eq. (3)	$-T_l R\ln K_{Lg}$
0–2–2	13.0	7.5	−19.87	−3.000	−19.06
			−19.86		
0–2–6	13.0	7.6	−19.87	,,	,,
			−19.86		
0–2–10	14.0	7.9	−19.82	−4.000	−19.78
			−21.2		
5–2–2	15.0	6.4	−20.24	−3.000	−19.19
5–2–6	12.1	6.7	−20.0	,,	−18.99
5–2–10	14.5	7.0	−20.0	−4.000	−19.81
			−23.7		
10–2–2	13.5	5.9	−20.52	−3.000	−19.09
10–2–6	13.2	6.1	−20.52	,,	,,
10–2–10	14.1	6.4	−20.34	−4.000	−19.79
			−21.75		
5–1–2	14.9	6.4	−20.2	6.000	−20.83
5–1–6	15.6	6.6	−20.2	,,	,,
5–1–10	15.8	6.5	−20.5	,,	,,
10–1–2	14.9	5.8	−20.6	,,	,,
10–1–6	14.8	6.0	−20.6	,,	,,
10–1–10	14.9	5.9	−20.6	,,	,,

Table 3
Determined parameters for Langmuir adsorption isotherms depending on water column height and air flow for the water column 2 m high—molar monolayer volume of chemisorbed oxygen V^{θ} $(O_{2,ch})_G = 1/c_a$ $(O_{2,ch})_g$—difference between oxygen chemisorption entropy to Langmuir adsorption isotherm $R\ln K_{Lg}$ and stationary liquid water entropy, S^{θ} (H_2O)

	$V^{\theta}_{mn}\ \frac{dm^3}{mol}$	$(R\ln K_{Lg}(O_2) - S^{\theta}(H_2O))\frac{J}{molK}$
c–1–*q*	6.0E22	$\frac{\Delta S^{\theta}(H^-)_{aq}}{2}$
except reg.		$72.3 - \frac{69.9}{2} = 2.4$
5–1–6		
c–2–*q* ⩽ 6 m^3/h	1.0E23	$66.6(reg.\ 0-2-q)$
		$66.6(reg 5-2-q;\ \text{and}\ :0-2-q)$
		$-\frac{\Delta S^{\theta}(H^-)_{aq}}{2}$
		$66.6 - \frac{69.9}{2} = -3.3$
c–2–*q* = 10 m^3/h	4.0E274	$\frac{\Delta S^{\theta}(H^-)_{aq2m}}{2} - \frac{(\Delta S^{\theta}(H^-)_{aq1m}}{2}$
		$68.9 - 69.9 = -1$

$$K_{couple} = \frac{([O_2]^* - [O_2]_s)}{[O_2]_s[e]\cdot[H^+]} \tag{5d}$$

The influence of dominant characteristics of adsorption centers is examined on the basis of Kelvin equation defining equilibrium:

- of fastest achieved equilibrium chemical potential, $\mu_{H_2} dn_a d\mu_{H_2} = dn_a V^{\theta} dp$

$$\Delta\mu_{H_2} = RT\ln\frac{p}{p_a} \tag{6}$$

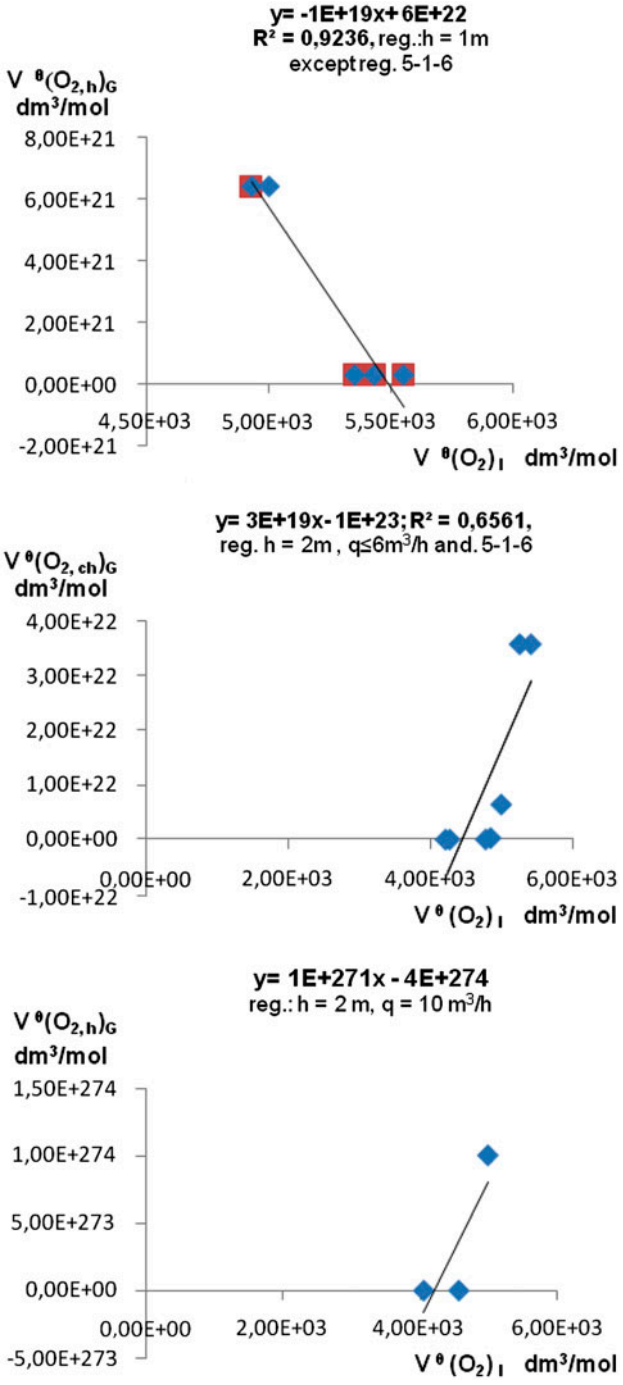

Fig. 2. Adsorption isotherms for examined aeration regimes based on the experimental data (Tables 1 and 2).

- on contact surface of gas bubbles and condensation or adsorption nucleuses radius r and liquid phase surface tension, σ:

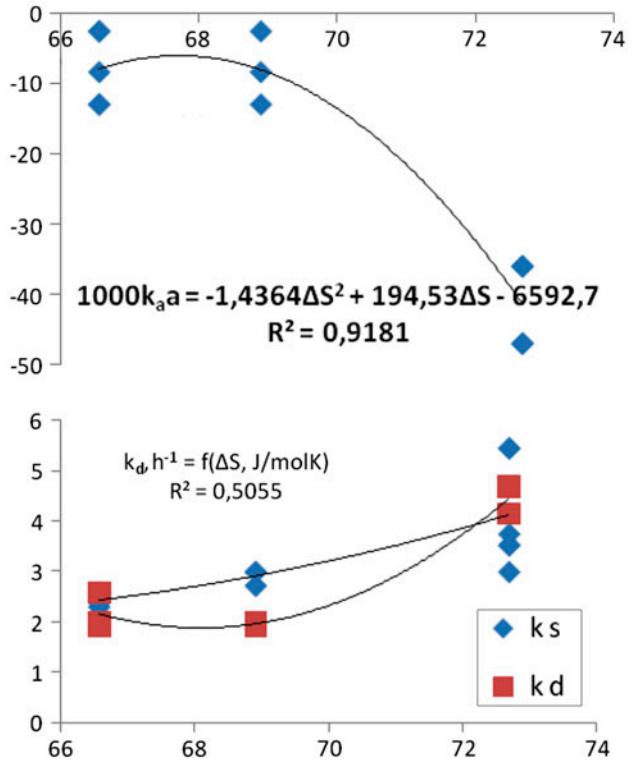

Fig. 3. The significant functionally dependence of oxygen adsorption entropy change, $R\ln K_{Lg} = \Delta S$ and electrons adsorption rate constant $1{,}000k_a$, as well as less significant on oxygen diffusion, k_d and oxygen saturation rate constant, k_s.

$$\Delta\mu_{H_2} = \sigma(4\pi(r-dr)^2 - 4\pi r^2)$$
$$\Delta\mu_{H_2} = 8\pi\sigma r dr \quad (7)$$

The experiments in literature showed that Kelvin equation corresponds to the measured values of condensation drops adsorption nucleuses with radius greater than 100 nm which corresponds to water vapor pressure of planar liquid surface.

In real system over-cooling decrease increased water molecules vapor pressure in smaller gas bubbles–crystallization nucleuses. Radius of n moles of adsorbed over-cooled hydrogen ($M_r = 2$ g/mol) with density ρ and surface tension, σ enable by equal mass of press-out liquid water drop, to Archimedes law acc to Eq. (7) relaxation of adsorbed oxygen over-pressure to be achieved:

$$dn_a M_{H_2O} = \rho_{H_2O} 4\pi r_{H_2O}^2 dr_{H_2O}$$
$$r_{H_2O} dr = \frac{dn_a M_{H_2}}{\rho_{H_2O}\pi r_{H_2O}} \quad (8)$$

Combined Eqs. (7) and (8) enable radius of adsorption nucleuses to be calculated (Table 5):

Table 4
Experimental data, air over pressure and oxygen active and passive rate constants previously determined, used to examine dominant influence on oxygen adsorption entropy change—saturation rate constants, k_s—mechanical and electrochemical relaxation rate constant, k_La [1,2]—diffusion rate constant, k_d [3]—oxygen adsorption rate constant, $1{,}000k_a.a$ [3]—measured air over-pressure, Δp_{air} [1,2]—oxygen desorption rate constant calculated in this paper to Eq. (1b), k_{des}

Reg. *c–h–q*	k_s h^{-1}	k_La h^{-1} [1,2]	k_d h^{-1}	10^3k_aa h^{-1} [3]	$\Delta p_{air\ in}$. N/dm^2 [2]	k_{des} h^{-1}
0–2–2	2.4	2.51	2.58	−13	212.7	4.3E–6
0–2–6	2.4	2.66	2.58	,,	239.2	,,
0–2–10	2.7	4.68	2.58	,,	333.2	3.2E–6
5–2–2	2.3	2.04	1.92	−8.4	218	2.8E–6
5–2–6	2.5	2.03	1.92	,,	273	,,
5–2–10	3.0	4.06	1.92	,,	3.2	2.1E–6
10–2–2	2.4	1.75	1.8	−2.6	231.3	8E–7
10–2–6	2.6	1.89	1.8	,,	263.1	,,
10–2–10	3	2.29	1.8	,,	321.5	6E–7
5–1–2	3.2	2.86	4.7	−47	135.5	−7.8E–6
5–1–6	3.5	3.74	4.7		170.1	,,
5–1–10	5.4	4.83	4.7		244.4	,,
10–1–2	3.0	2.34	4.16	−36	135.5	−6E–6
10–1–6	3.7	3.11	4.16		167.4	,,
10–1–10	5.4	3.95	4.16		244.4	,,

Table 5
Characteristics of condensation nucleuses calculated to Langmuir adsorption isotherm, Eq. (2) and Kelvin equation (10) and energy efficiency of oxygen transport used in previous papers [2,4]—monolayer oxygen concentrations, $c(O_{2ad\ max})_g$—number of active centers in molar vonolayer volume, $N_Ac_{ad\,max}$—radius of adsorption nucleuses depending on aeration regimes calculated to Eq. (10)—energy efficiency of oxygen transport obtained previously [1,2]

c–h–q	$c(O_{2ad\ max})_g$ mol/dm^3 Eq. (2a)	$N_Ac_{ad\,max}$	*r*, nm Eq. (10)	*E*, e g/kWh
0–2–2	1E−23	6	6,1	35.1
0–2–6	,,	,,	5,5	15.0
0–2–10	2.5E−275	0	4	14.8
5–2–2	1E−23	6	4,9	28.4
5–2–6	,,	,,	4,4	11.5
5–2–10	2.5E−275	0	978,5	13
10–2–2	1E−23	6	4,3	24.5
10–2–6	,,	,,	3,8	10.7
10–2–10	2.5E−275	0	3,2	7.3
5–1–2	1.7E−23	10	7,8	18.4
5–1–6	1E−23	6	6,3	9.8
5–1–10	,,	10	4,6	7.06
10–1–2	,,	,,	6,9	15
10–1–6	,,	,,	5,6	8.09
10–1–10	,,	,,	4	5.8

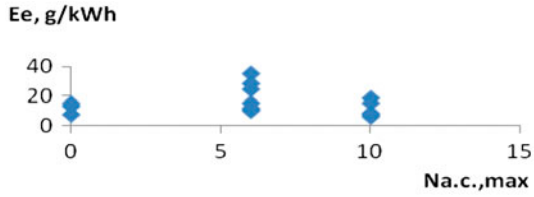

Fig. 4a. The examination of catalytic influences of the maximal number of the condensation nucleuses in molar volume, N_{max} = const., on the energy efficiency of oxygen introduction, Ee depending on the examined aeration regimes, *c–h–q*.

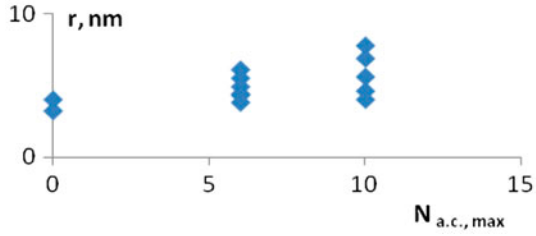

Fig. 4b. The correlation of the radiuses of adsorption and condensation nucleuses, r with the number of condensation nucleuses, N_{max}.

$$RT\ln\left(\frac{p_{in}}{p_o}\right)_{H_2} = \frac{2\sigma M_{H_2}}{\rho_{H_2O}\cdot r_{H_2O}} \tag{9}$$

$$r_{H_2Oac} = \frac{2\sigma_{H_2O} M_{H_2O}}{\rho_{H_2O} RT_l \ln\frac{p_{in}}{p_a}}$$
$$r_{H_2Oac} = 15,1\cdot 10^{-9}\frac{\sigma_{H_2O}}{\ln\frac{p_{in}}{p_a}} \tag{10}$$

Energy efficiency of oxygen transport depend on maximal number of condensation nucleuses in molar volume, $N_{a.c.max}$ and show the catalytic influence:

- for $N_{a.c.max} = 6$ (see Fig. 4a).
- in the range of radiuses of adsorption and condensation nucleuses, r: 3,8 nm < r < 6,1 nm (see Fig. 4b),
- at r = 6,1 nm for regime without added waste motor oil, c = 0 in 2 m high water column at minimal air flow, 2 m3/h(0-2-2), according to the obtained maximal slope for the linear functional dependence of energy efficiency of oxygen transport, Ee on the radius of adsorption and condensation nucleuses, r t_g = 5,845, in comparison to the other examined functional dependences where, t_g = 2,6 −3,5 (see Fig. 4c).

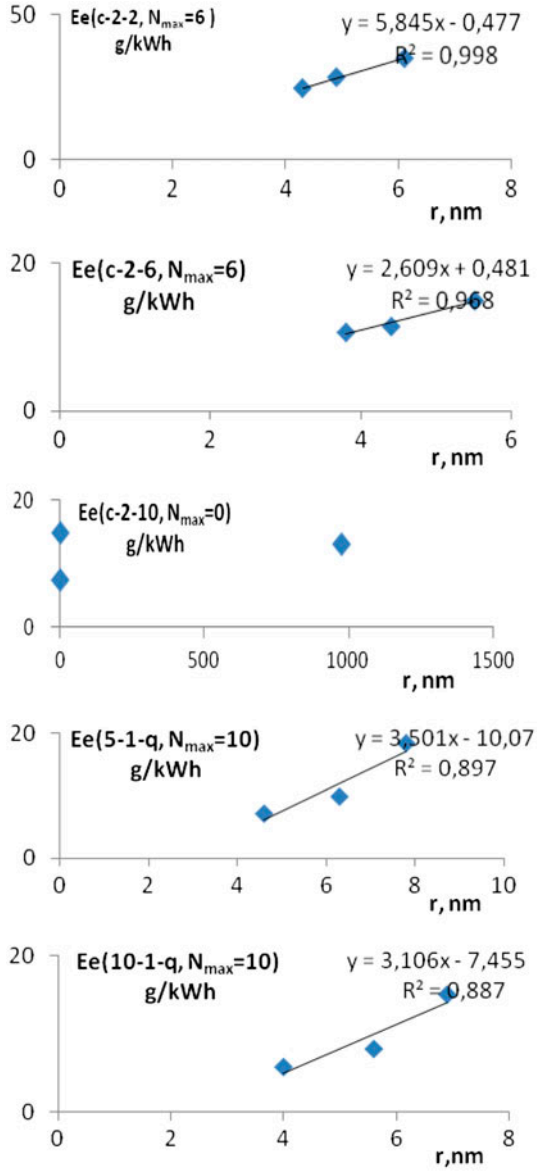

Fig. 4c. The functional dependences (R_2 = 0.89–0.99) of the energy efficiency of oxygen introduction, Ee on the radiuses, r: for 2 m high water column (*c–2–q*), at N_{max} = const and at constant value of air flow, q as well as for 1 m high water column (c–1–q), at N_{max} = const. and at constant value of added oil content, c.

4. Potential difference between planar water surfaces on air input and output

Potential difference between planar water surfaces on air input and output, ΔU determine the total diffusion polarization of water column dielectric barrier depending on oxygen molar adsorption affinity:

Table 6
Potential difference between planar water surfaces on air input and output calculated on the base experimental data presented in Tables 1 and 2, calculated to Eqs. (11) and (11a)

Δc–h–q	$\eta(O_2)_g = -\frac{\Delta G(O_2^-) \pm F\eta_d(O_2)_G}{F}$	$\pm\eta_d(O_2)_L$, V	$\Delta U(O_2)$ V Eq. (12)
0–2–2	*0.2* ($HO_2^- + OH^- = O_2^- + H_2O + e$) $= T\Delta S_{H_2O}/F$	0.2	0
	0.943	0.2	0.4
	($O_3 + H_2O + e = O_2 + OH + OH^-$)		0.74
			1.14
0–2–6	,,	,,	,,
0–2–10	*0.2* ($HO_2^- + OH^- = O_2^- + H_2O + e$) $= T\Delta S_{H_2O}/F$	0.2	0
	13.76 ($OH = OH^+ + e)_G = f(\leqslant 2U_L$(NaCl) = 1.557;	0.2	0.4
	ΔH^θ ($H_2C = CH_2 + 4O_2 = 2CO_2 + 2H_2O$)	2	−13.5
	= −1.386 kJ/mol)		−14
5–2–2	−1.26 ($O_3 + H_2O + 2e = O_2 + 2OH^-$)	0.21	−1.05
			−146
5–2–6	−1.14 ($H_2O_2 + H^+ + e = H_2O + OH$)	0.21	−1.14
			−1.35
5–2–10	$-0.38 = f(\Delta_s H^\theta$(NaCl)=$O_3 + H_2O + 2e$	0.21	−0.17
	$= O_2 + OH^-) \leqslant 2U_L$ (NaCl) = 15.57	0.2	−0.58
	13.76 ($OH = OH^+ + e)_G$	4	−13.5
	=f(ΔH^θ ($H_2C = CH_2 + 4O_2 = 2CO2 + 2H_2O$)		−14
	= −1.386 kJ/mol)		
10–2–2	$-1.14 = (H_2O_2 + H^+ + e = H_2O + OH$)	0.21	−0.93
			−1.35
10–2–6	"	0.21	"
10–2–10	$-$***1.23*** $(O_3)_{aq}$	0.21	−1
	13.76 = f($2U_L$(NaCl) = 1.557 = f(ΔH^θ ($H_2C = CH_2 + 4O_2 = 2CO_2 + 2H_2O$) = −386 kJ/mol)	0.22	−1.43
			−14
5–1–2	*−1.26* ($O_3 + H_2O + 2e = O_2 + 2OH^-$)	0.21	−1
			−1.47
5–1–6	*0.943* ($O_3 + H_2O + e = O_2 + OH + OH^-$)	0.21	1.1
			0.73
5–1–10	*−1.26* ($O_3 + H_2O + 2e = O_2 + 2OH^-$)	0.21	−1.05
			−1.46
10–1–2	*−1.23* ($O_3 + H_2O + 2e = O_2 + 2OH^-$)	0.21	,,

$$\Delta U(O_2) = \eta_d(O_2)_g \pm \eta_d(eH_2O)_L \quad (11)$$

$$\eta(O_2)_g = -\frac{\Delta G(O_2^-) \pm F\eta_d(O_2)_G}{F} \quad (11a)$$

The presence of Ohms polarization of condensation and adsorption nucleuses, I_eR_{Ohm} influence on oxygen isobaric over-pressure potential difference between planar water surfaces on air input and output al, $\eta(\Delta p)$:

$$\Delta U(O_2) = \eta(\Delta p) + I_eR_{Ohm} \quad (12)$$

Potential difference between planar water surfaces on air input and output are calculated on the basis of experimental data presented in Tables 1 and 2.

The obtained results agree to the standard potentials of oxygen reduction reactions, according to literature [5] (Table 6):

- Direct oxygen reduction without forned intermediere:

$$E^\theta(O_2 + H_2O + 4e^- = 4OH^-)0.401\ V$$

Table 7
The calculated data for oxygen electrochemical relaxation rate constant, k_{ePLTE} enabling relaxation of oxygen adsorption affinity as well as of monolayer relative electric permittivity enabling relaxation of oxygen over pressure, depending on surface plasma electrons density—oxygen electrochemical relaxation rate constant, k_{ePLTE}—surface plasma electrons density change, $[e,\mathrm{H}^+]_r$—electrons adsorption affinity $\frac{\Delta_a G^\theta(\mathrm{O}_2)}{[e]_r}$—monolayer relative electric permittivity enabling relaxation of oxygen over pressure, $\varepsilon_r(\Delta p)$—electrochemical over-pressure relaxation over-potential, $\eta(\Delta p)$

Reg. *c–h–q*	k_{ePLTE}, h^{-1}	$[e,\mathrm{H}^+]_r$, moldm^{-6}	$\frac{\Delta_a G^\theta(\mathrm{O}_2)}{[e]_r}$, $\mathrm{J/mo^2dm^{-6}}$	$\varepsilon_r(\Delta p)$	$\eta(\Delta p)$, V
0–2–2	0.77	59	515	27.3	0.65
			−638	33.8	0.81
0–2–6	0.74	57	533	25.1	0.6
			−637	30	0.7
0–2–10	0.949	73	416	14	0.33
			−18.863	634	15.2
5–2–2	1.1	132	−564	61.2	1.46
5–2–6	1.09	130	−494	53.6	1.29
5–2–10	0.86	102	−629	4.765	1.14
			−13.500	1E5	2.400
10–2–2	0.72	278	−231	49	1.18
10–2–6	0.72	278	−231	43	1.03
10–2–10	0.94	360	−196	30	0.72
			−3.825	585	14.04
5–1–2	90	1.925	−38.7	6.8	0.16
5–1–6	98.7	2.100	−17.3	2.4	0.058
5–1–10	97.9	2.083	−35.7	3.5	0.084
10–1–2	111	3.111	−22.7	8.2	0.20
10–1–6	117.7	3.270	−21.6	6.3	0.15
10–1–10	114.8	3.185	−22.2	4.4	0.1

- Indirect oxygen reduction with formed intermediere hydroperoxyde:

$$\mathrm{E}^\theta(\mathrm{HO}_2^- + \mathrm{H_2O} + 2e^- = 3\mathrm{OH}^-) = 0.88\,\mathrm{V}\,\mathrm{E}^\theta$$

$$(\mathrm{HO}_2^- + \mathrm{OH}^- = \mathrm{O}_2^- + \mathrm{H_2O} + e) = 0.2\,\mathrm{V}$$

$$\mathrm{E}^\theta(\mathrm{H_2O_2} + \mathrm{H}^+ + e = \mathrm{H_2O} + \mathrm{OH}) - 1.14\,\mathrm{V}$$

- Coupled process [3]:

$$\mathrm{O_2} + \mathrm{e} = \mathrm{O_2}\ \mathrm{E}^\theta = 0.33\,\mathrm{V}$$

$$\mathrm{O}_2^- + \mathrm{H}^+ = \mathrm{HO_2E}^\theta = 0.12\,\mathrm{V(pK = 4.8)}$$

$$\mathrm{O_2} + \mathrm{e} + \mathrm{H}^+ = \mathrm{HO_2}\Delta G_{couple} = \Delta G_1 + \Delta G; \sum \Delta\chi^\theta = \pm 0.46\,\mathrm{V}$$

5. Electrochemical relaxation processes rate constant

Relaxation processes in contact surface between the two phases determine equal power in the both gas and liquid phase depending on:

- oxygen electrochemical relaxation rate constant, k_{ePLTE}.
- surface plasma electrons density change $[e,\mathrm{H}^+]_r$ calculated in previous paper [4].

Coupled oxygen monolayer chemisorptions to Langmuir adsorption isotherm and plasma surface electrons [4] enable relaxation of molar oxygen adsorption affinity, $\Delta_{a,e}G^\theta(\mathrm{O_2})$ to thermal energy 3RT, depending on electrochemical relaxation rate constant, k_{ePLTE}:

$$k_a \cdot [e,\mathrm{H}^+]_r 3RT = k_{ePLTE}\Delta_{a,e}G^\theta(\mathrm{O_2}) \tag{13}$$

when electrochemical relaxation rate constant of surface plasma electrons achieve the value:

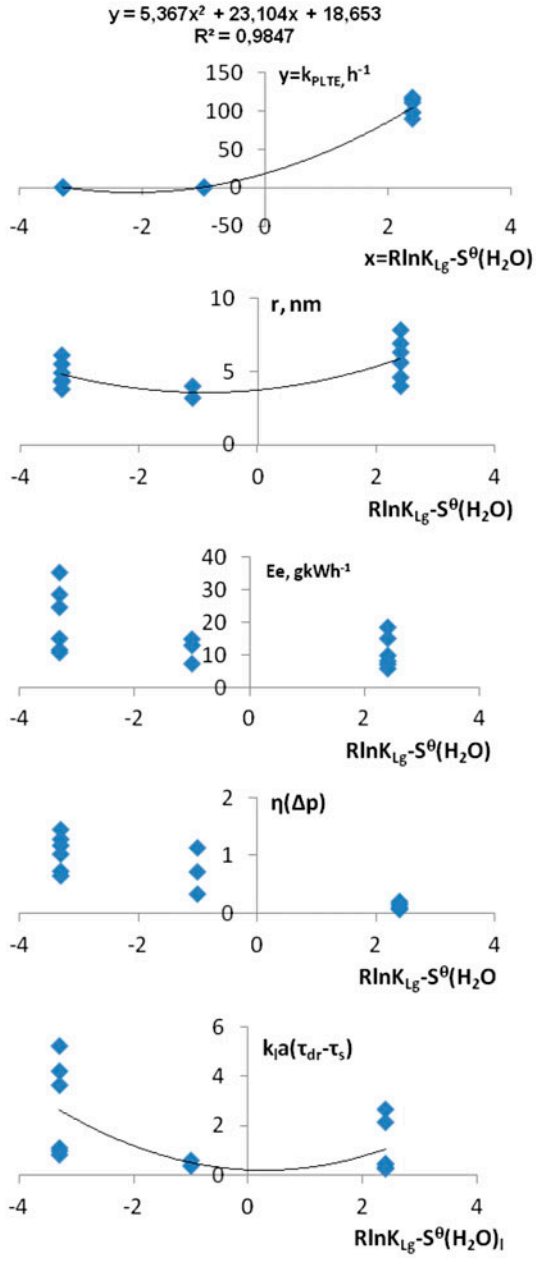

Fig. 5. The examined correlation with aim to define dominant parameters in oxygen electrochemical relaxation processes enabling isothermal isobaric oxygen dissolution in liquid phase.

$$k_{ePLTE} = k_a \cdot [e]_r \tag{13a}$$

Oxygen adsorption power in isochoric liquid monolayer layer in contact surface between gas and liquid phase has to be equal to electrons transport energy for achieving stationary oxygen surface over-pressure work in gas phase:

$$k_{ePLTE}\frac{V^{\theta}\Delta p}{\varepsilon_o} = k_a\frac{RT}{2\varepsilon} \tag{14}$$

On solving Eq. (14) give relative electric permittivity of dielectric barrier enabling electrons transport energy determining oxygen surface over-pressure work in gas phase:

$$\varepsilon_r(\Delta p) = \frac{k_a}{k_{ePLTE}}\frac{RT}{2V^{\theta}\Delta p} \tag{15}$$

Combining with Eq. (13) give:

$$\varepsilon_r(\Delta p) = \frac{1}{6}\frac{\Delta_{a,e}G^{\theta}(O_2)}{[e,H^+]_r V^{\theta}\Delta p} \tag{16}$$

Electrochemical over-pressure relaxation over-potential determine diffusion energy transfer in air depending on monolayer electric permittivity, ε determined to Eq. (16):

$$\frac{F\eta(\Delta p)}{\varepsilon} = \frac{RT}{\varepsilon_0} \tag{17}$$

$$\eta(\Delta p) = \varepsilon_r(\Delta p)\frac{RT}{F} \tag{18}$$

Calculated electric permittivity of active adsorbed centers are compared with relative electric permittivity defined to literature [21] for Helmholtz planes double layer in contact surfaces with specifically and un-specifically adsorbed particles:

- $\varepsilon_r = 6$ for inner Helmholtz plane (IHP)
- $\varepsilon_r = 30$ for outer Helmholtz plane (OHP)
- $30 < \varepsilon_r < 80$ for diffusion layer

The obtained results of electrochemical over-pressure relaxation over-potential, $\eta(\Delta p)$, depending on the monolayer relative electric permittivity, show the difference in the thermodynamic history of oxygen adsorption heat (see Table 7):

- for water column 2 m high, after the isochoric relaxation of oxygen chemical potential is achieved on air input, successive isobaric over-pressure enable oxygen electrochemical relaxation.
- for water column 1 m high, after isobaric over-pressure electrochemical oxygen relaxation at lower values compared to water column 2 m high, isochoric processes enable relaxation of dissolved oxygen chemical potential.

Dominant influence on the oxygen electrochemical relaxation rate constant are examined on the basis of correlations in Fig. 5.

The best correlation coefficient is found for functional dependence between electrochemical rate constant and water entropy level (defined in Table 3 as difference between adsorption oxygen entropy to Langmuir adsorption isotherm and liquid water entropy), $R^2 = 0.987$:

$$k_{ePLTE} = 5.367\Delta S\theta^2(H_2O) + 23.104 + \Delta S\theta(H_2O) + 18.653$$

The correlation between the positive or negative difference between adsorption oxygen heat and liquid water entropy and electrochemical relaxation rate constant, k_{ePLTE} influence on the energy efficiency of oxygen transport.

The obtained results show:

- negative value of entropy change on contact surface between the smallest gas bubbles and liquid cause the smallest electrochemical isobaric relaxation rate constant after isochoric achieved over-pressure and increased energy efficiency for water column 2 m high (and increased stationary over-pressure and molar oxygen level energy between drift and saturation period).
- on contact surface between the increased radius of the gas bubbles and liquid, positive value of entropy change cause decreased energy efficiency (and decreased stationary over-pressure and molar oxygen level energy between drift and saturation period) for water column 1 m high at lower isobaric over-pressure relaxation rate constant for water column 1 m high.

6. Conclusion

Positive or negative liquid water entropy change the influence dominant on the oxygen electrochemical relaxation rate constant and energy efficiency of oxygen transport, depending on aeration column height:

- in water column 2 m high where previous isochoric over-pressure relaxation of chemical potentials negative entropy change enable successive isobaric over-pressure to be achieved, on air output planar contact surfaces between liquid and air also controlling oxygen transport work and electrochemical relaxation rate constant.
- in water column 1 m high, the previous lower isobaric isothermal transport work control electrochemical relaxation rate constant and successive isochoric positive entropy change on air output.

References

[1] M. Stanojević, D. Radić, S. Simić, Determining the technical characteristis of the aeration systems for oil refinery, s waste water treatment, in: 16th International Congress of Chemical and Process Engineering, CHISA, Praha, Czech Republic, 22.-26.08, 2004, pp. 3863–3873.
[2] Determination the technical characteristics of N.S. Simic, Influence of the Aeration System Solution on Efficiency of Biology Treatment of Refinery Waste Water, Ph.D. Thesis, Faculty of Mechanical Engineering, University in Belgrade, 2006.
[3] M. Ševaljević. M. Stanojević, S. Simić, M. Pavlović, Thermodynamic Study of Aeration Kinetic in Treatment of Refinery Wastewater in Bio-aeration Tanks, Desalination 248 (2009) 941–960.
[4] M. Mirjana, M. Ševaljević, N. Stojan, S. Simić, V. Petar, M. Ševaljević, Thermodynamic Diagnostic of Electron Densities in Gas Bubbles in Aerated Saturated Refinery Waste Water, Desalination and Water Treatment, in press adapted December 6. 2011.
[5] A. Bard, R. Parsons, J. Jordan, Standard Electrochemical Potentials in Aqueous Solutions, JUPAC ed., Base, New York, 1983.
[6] J. Cohen, K. Schulten, Mechanism of Anionic Conduction Across ClC, Biophysical Journal 86(2) (2004) 836–845.
[7] K. Egan-Benck, G. McCarty, W. Winkler, Choosing Diffusers, Water Environment and Technology 5(2) (1993) 54–59.
[8] K. Fujie, K. Tsuchiya, L. Fran, Determination of Oxygen Transfer Coefficient by Off-Gas Analysis, Journal of Fermentation and Bioengineering (1994).
[9] J. Mc Whirter, J. Hutter, Improved Oxygen Mass Transfer Modeling For Diffused/Sibsurface Aeration Systems, Department of Chemical Engineering, The Pennsylvania State University Park, PA 16802, AIChE Journal 35(9) (1989) 1527–1534.
[10] R. Mc Gregor, Diffusion and sorption in Fibres and Films, Fiber Chemistry, Marcel Dekker, vol. 1, New York, 1973.
[11] K. Ashley, K. Hall, D. Mavinic, Factors Influencing Oxygen Transfer in Fine Pore Diffused Aeration, University of British Columbia, Water Research, vol. 25, Vancouver, 1998, pp. 1479–1486.
[12] M. Wagner, J. Pöpel, Oxygen Transfer and Aeration Efficiency–Influence of Diffuser Submergence, Diffuser Density and Blower Type, in: Water Quality International, IAWQ 19th Bienial international Conference, Vancouver, Canada, 1998.
[13] H.J. Simičić, The processes in treatment of the waste water, Tuzla 2002.
[14] H.J. Rehm, G. Reed, W. Schonborn, Microbial Biotechnology, Volume 8, Microbial Degradation, VCH Verlagsgesellschaft mbH, Weinheim, 1986.
[15] K.A. Tay, F.X. Coudert, A. Boutin, Mechanism and Kinetics of Hydrated Electron Diffusion, The Journal of Chemical Physics 129 (2008) 054505.
[16] K.H. Scmidt, P. Hahn, D.M. Bartels, Journal of Physical Chemistry 99 (1995) 10530.
[17] I. Prigogine, Introduction to Thermodynamics of Irreversible Processes, Wiley, New York, 1967.
[18] S. Mentus, Electrochemistry, 2nd ed., University in Belgrade, 2001.
[19] A.T. Fromhold, Jr., E.L. Cook, Kinetic of Oxide Film Growth on Metal Crystals: Electron Tunneling and Ionic Diffusion, Physical Review 158(Nb3) (1967) 600–612.
[20] G. Alain, H. Kafrouni, H. Dang Duc, C. Maury, The difference between the electron temperature abd the gas temperature in a stationary arc at atmospheric pressure, Journal of Physics D: Applied Physics 15 (1982) 1031–1045.
[21] H.B. Mark, Jr., Electrocatalysis and its Application to Analysis, Analyst, 115(6) (1990) 667.